Laser-induced Fluorescence Study of Neutral Xenon Flow Evolution inside a 6-kW Hall Thruster

IEPC-2009-087

Presented at the 31st International Electric Propulsion Conference, University of Michigan • Ann Arbor, Michigan • USA September 20 – 24, 2009

Wensheng Huang[*] and Alec D. Gallimore[†]
Plasmadynamics and Electric Propulsion Laboratory, University of Michigan, Ann Arbor, MI 48109, USA

We present laser-induced fluorescence velocimetry measurements obtained using the Xe I 6s[3/2]$^0_2$ → 6p[3/2]$_2$ transition at 823.4 nm (vacuum) and the Xe I 6s'[1/2]$^0_1$ → 6p'[3/2]$_2$ transition at 834.9 nm (vacuum) from the inside and in the near-field plume of a 6-kW Hall thruster. The thruster is operated under seven conditions with discharge voltages ranging from 150 to 600 V, and anode mass flow rates ranging from 10 to 30 mg/s. Axial sweeps along channel centerline are performed at each operating conditions. Radial sweeps at the exit plane are performed at the nominal condition. Velocimetry results show that the neutral propellant starts at a bulk velocity of ~100 m/s at the anode and accelerates to 300-400 m/s by the exit plane. Temperature of the neutrals starts out high (1000-1600 K) near the anode but cools down to 500-800 K near the exit plane. Rapid changes in the strength of the collected fluorescence during the axial sweeps allowed the identification of the approximate ionization zone locations. The anode mass flow rate appears to have a bigger influence on the bulk velocity and temperature of the neutrals than the discharge voltage. Radial sweeps revealed the possible presence of near-wall boundary layers approximately a few mm thick. Implications of these results for Hall thruster physics are discussed.

I. Introduction

MANY Hall thruster studies traditionally start with electrostatic probe measurements because probes are relatively low-cost, robust, and relatively straightforward to use. However, electrostatic probes, by nature, cannot obtain any information about the neutral flow in a Hall thruster. This gap in knowledge is typically bridged with fluid or particle simulation. Yet, several studies in the past have shown that neutral flow mechanics can play a very important role in controlling the location and properties of the plasma in a Hall thruster.[1, 2] Due to a lack of neutral flow data, it is difficult to judge the fidelity with which neutral flow behavior is captured in simulations. Laser-induced fluorescence (LIF) presents a unique technique for bridging the knowledge gap in that it is non-intrusive, species-specific, and capable of extracting information about the neutrals in the Hall thruster discharge channel. There have been several previous neutral flow studies using LIF[3, 4] including internal flow measurements obtained through a slot in the channel.[5] This paper will present neutral flow data inside and near the exit plane of a 6-kW Hall thruster operating on xenon. The data are obtained without the use of a slot and is truly non-intrusive. Extraction of velocity distribution functions from LIF spectra is explained; followed by a discussion of the results and physical trends found, and a discussion of the physical implications of the results.

Two LIF experiments will be described in this paper; the first experiment is carried out using the Xe I 6s[3/2]$^0_2$ → 6p[3/2]$_2$ transition at 823.4 nm (vacuum), while the second experiment is carried out using the Xe I 6s'[1/2]$^0_1$ → 6p'[3/2]$_2$ transition at 834.9 nm (vacuum). Two different types of spatial sweeps are carried out. The axial sweeps along the channel centerline revealed how the neutral flow bulk velocity and temperature evolved as the flow moved

[*] Ph. D. Candidate, Aerospace Engineering, davhuang@umich.edu.
[†] Arthur F. Thurnau Professor, lab director, Aerospace Engineering, Alec.Gallimore@umich.edu.

downstream from the anode into the near-field. The radial sweeps across the exit plane of the thruster revealed the difference between neutral flow near the walls and on centerline.

II. Theories

Subsections A and B lay out the theory underlying the extraction of velocity distribution functions (VDF) from raw LIF spectra. Subsection C briefly discusses the differences between continuum and free-molecular flows as well as the velocity profile and temperature trends associated with each type of flow. For the remainder of this paper, all transition wavelengths are given in vacuum values and all intensities given in arbitrary units, a.u., unless otherwise specified.

A. Principles of Laser-Induced Fluorescence Velocimetry

LIF velocimetry operates on the principle that a particle (an atom or molecule) absorbs a photon at a shifted frequency when moving due to the Doppler Effect. The particle has a chance of spontaneously emitting a photon when it de-excites. This spontaneous emission, called fluorescence, radiates isotropically away from the particle. For a particle travelling at non-relativistic speed, the shift in absorption frequency is proportional to the particle velocity component in the direction that the photon travels. The mathematical equation is given in Eq. (1),

$$\frac{\Delta\upsilon}{\upsilon_0} = -\frac{\mathbf{v}}{c}\cdot\frac{\mathbf{k}}{|\mathbf{k}|} \tag{1}$$

where υ_0 is the photon frequency, $\Delta\upsilon$ is the shift in photon frequency from the perspective of the particle, $\mathbf{v}$ is the particle velocity, c is the speed of light, and $\mathbf{k}$ is the photon wave vector. By varying the frequency of the injected photons and comparing the intensity of the collected fluorescence, we can obtain the particle VDF along the injected photon wave vector.

In the first experiment, light is injected at 823.4 nm and the fluorescence is collected at the same wavelength. This type of LIF is described as being resonant. In the second experiment, light is injected at 834.9 nm and the fluorescence is collected at 473.5 nm. This type of LIF is described as being non-resonant. Figure 1 shows the associated transition diagram. A non-resonant collection scheme does exist for injection at 823.4 nm in which fluorescence is collected at 895.5 nm (the lower state is $6s[3/2]^0{}_1$). However, traces taken separately with an optogalvanic cell show that the signal for this non-resonant collection scheme is three orders of magnitude lower than that for the resonant collection scheme.

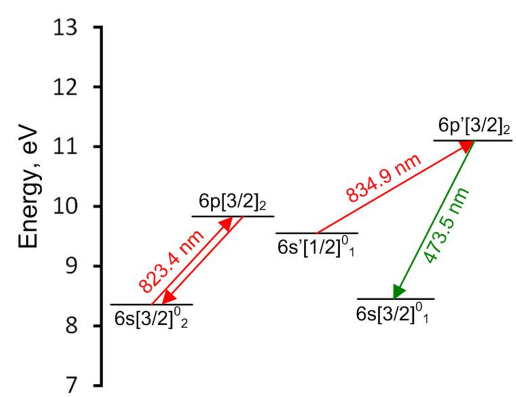

Figure 1. Transition diagram for the two experiments. ***Wavelengths in vacuum*.**

The reason why two transitions are used to probe the neutral flow is because each has its own advantages and disadvantages. The lower state of the Xe I 823.4 nm transition is metastable and the signal is exceptionally strong; so strong that this line is typically highly saturated under most experimental conditions. A transition line is saturated when the associated upper state particles do not have enough time to de-excite before they are stricken by other photons. An easily saturated line is useful for measuring relative particle density because the fluorescence signal becomes insensitive to input laser power. However, the saturation effect leads to broadening that distorts the lineshape so that only peak velocity can be extracted from a saturated Xe I 823.4 nm lineshape. Furthermore, since the 823.4 nm LIF scheme is resonant the signal can be distorted by scattering of light on thruster internal surfaces making it impossible to collect data too close to the walls and the anode.

The 834.9 nm LIF scheme described earlier has the advantage of being non-resonant and can be used to probe near the thruster walls and the anode. However, the associated lower state is not metastable and the signal tends to be weaker than the 823.4 nm LIF scheme. It is relatively easy to obtain unsaturated lineshapes with the 834.9 nm LIF scheme so velocity distribution functions can be obtained.

Note that in these two LIF experiments the measured quantities are of the initial excited states, which is assumed to have the same VDF as the entire neutral population.

B. Hyperfine Structure and Natural Broadening

The FWHM of the average neutral VDF in a Hall thruster typically varies from 400 to 800 m/s, which for a near-infrared transition corresponds to about 500 to 1000 MHz. Unfortunately, the xenon hyperfine structures for the two transitions used in this study is up to several GHz wide. These structures add large distortions to the raw data and must be removed if we want to get the velocity distribution functions.

Hyperfine structure arises primarily out of the coupling between the intrinsic electric and magnetic fields of the electrons and the nucleus in the atom. Paired nucleons have zero net spin because the spin vectors of nucleons in a pair tend to point in opposite directions. The atomic number of xenon is 54 so the number of protons is even. Of the nine stable isotopes of Xenon, only two (Xe-129 and Xe-131) have an odd number of neutrons. The energies of the otherwise degenerate states in these isotopes will shift slightly, leading to hyperfine structure. The shift in energy is described by Eq. (2),

$$E_{hfs} = A\frac{C}{2} + BD,\ C = F(F+1) - I(I+1) - J(J+1),\ D = \frac{(3C/4)(C+1) - I(I+1)J(J+1)}{2I(2I-1)J(2J-1)} \tag{2}$$

where A is the magnetic dipole interaction constant, B is the electric quadrupole interaction constant, I is the nuclear spin angular momentum quantum number, J is the total electron angular momentum quantum number, and F is the total resultant angular momentum quantum number and obeys Eq. (3). The selection rule for allowed transitions is in Eq. (4).

$$F = I+J, I+J-1, \ldots, |I-J| \tag{3}$$

$$\Delta F \equiv F_U - F_L = [0, \pm 1],\ F_L = 0 \nrightarrow F_U = 0 \tag{4}$$

In Eq. (4) F_L and F_U are the total angular momentum quantum numbers for the lower and upper states, respectively. The zero to zero transition is forbidden. For Xe-129 and Xe-131, I equals 1/2 and 3/2, respectively. Xe I 823.4 nm is a $J_L=2 \rightarrow J_U=2$ transition, while Xe I 834.9 nm is a $J_L=1 \rightarrow J_U=2$ transition, where J_L and J_U denotes the total electron angular momentum of the lower and upper states, respectively. The relative intensity for a $J \rightarrow J$ transition is given by Eqs. (5-7,11) [6] and for a $J\text{-}1 \rightarrow J$ transition by Eqs. (8-11).[7]

$$\mathrm{Int}(F \rightarrow F-1) \sim P(F)Q(F-1)/F \tag{5}$$

$$\mathrm{Int}(F \rightarrow F) \sim \frac{2F+1}{F(F+1)}[R(F)]^2 \tag{6}$$

$$\mathrm{Int}(F\text{-}1 \rightarrow F) \sim P(F)Q(F-1)/F \tag{7}$$

$$\mathrm{Int}(F \rightarrow F-1) \sim Q(F)Q(F-1)/F \tag{8}$$

$$\mathrm{Int}(F \rightarrow F) \sim \frac{2F+1}{F(F+1)}P(F)Q(F) \tag{9}$$

$$\mathrm{Int}(F\text{-}1 \rightarrow F) \sim P(F)P(F-1)/F \tag{10}$$

$$P(F) = (F+J)(F+J+1) - I(I+1);\ Q(F) = I(I+1) - (F-J)(F-J+1);\ R(F) = F(F+1) + J(J+1) - I(I+1) \tag{11}$$

On top of the nuclear-electron electromagnetic interactions, variations in nuclear mass and volume causes slight differences in electron orbital states. Each stable isotope of xenon has an associated shift in transitional energy described by the parameter called isotopic shift. The relative intensity of each transition is proportional to the abundance of the associated isotope. There are quantum models for isotopic shift, but the orbit calculations for an atom as complex as xenon is computationally prohibitively expensive so isotopic shifts for xenon are typically found by empirical methods. All together, the magnetic dipole constant, A, the electric quadrupole constant, B, and the isotopic shifts are commonly referred to as the hyperfine structure constants. The hyperfine structure constants for both the Xe I $6s[3/2]^0_2 \rightarrow 6p[3/2]_2$ and the Xe I $6s'[1/2]^0_1 \rightarrow 6p'[3/2]_2$ transitions are well established.[8-10]

Additionally, externally applied electric and magnetic fields can induce additional hyperfine splittings. These splittings depend on the direction and polarity of the injected laser beam. The splitting effect induced by an external electric field is called the Stark effect. The electric field present in a typical Hall thruster is several orders of magnitude smaller than what is necessary to cause a detectable frequency shift in xenon.[11] The applied magnetic field effect for weak field strengths (~100 G), called the Zeeman effect, can be categorized under σ- and π-polarization. The laser beam is σ-polarized if the polarization of the beam is perpendicular to the external magnetic field ($\mathbf{E} \perp \mathbf{B}$). The beam is π-polarized if the polarization of the beam is parallel to the external magnetic field ($\mathbf{E} \parallel \mathbf{B}$). For the Xe I 834.9 nm transition, π-polarized splittings are at least an order of magnitude narrower than σ-polarized splittings. By injecting the laser beam with a radial polarization to match the approximately radial magnetic field at the Hall thruster exit plane, we can obtain LIF scans with negligible Zeeman splitting.[12] Unpublished traces obtained with the same setup as Ref. 12 shows that the 823.4 nm transition behaves similarly.

Natural (or lifetime) broadening can be explained by the Heisenberg uncertainty principle. Since energy and temporal measurements are complementary, we cannot know with absolute certainty the exact energy of a photon emitted from a particle whose decay time is uncertain. The result is that even if all other circumstances are equal, no two photons from the same de-excitation will be measured with exactly the same energy. This effect broadens a transition line into a Lorentzian function. The lifetime constant for both of the transitions used in this study are known.[13] Figures 2a and 2b show simulated cold spectra for the Xe I 823.4 nm and 834.9 nm transitions, respectively. They also show simulated 600 K warm plasma spectra for each transition.

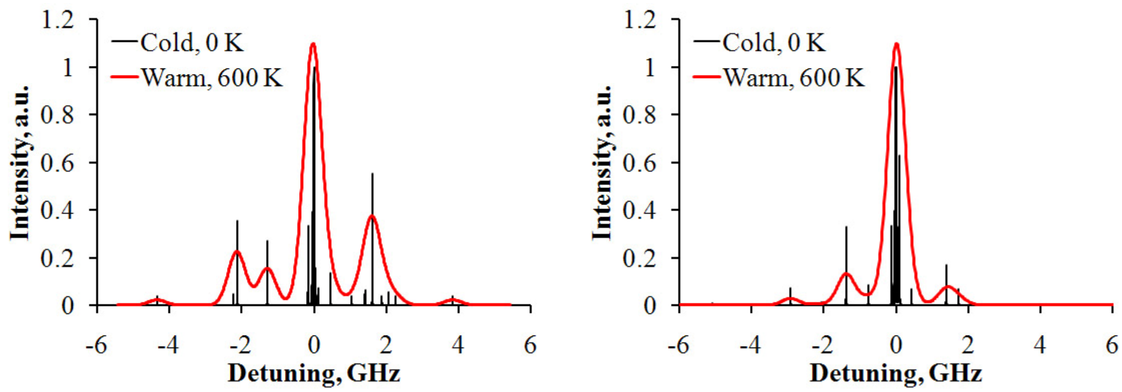

Figure 2. Simulated cold and warm hyperfine structure lineshapes for the Xe I 823.4 nm (sub-figure a, left) and 834.9 nm (sub-figure b, right) transitions. *Wavelengths in vacuum.*

C. Continuum versus Free Molecular Flow

The operating regime of the neutral flow can be determined by the Knudsen number as described in Eq. (12),

$$\begin{aligned} &\mathrm{Kn} \equiv \lambda / \mathrm{L} \\ &\mathrm{Kn} << 1, \text{ Continuum flow} \\ &\mathrm{Kn} >> 1, \text{ Free molecular flow} \end{aligned} \tag{12}$$

where λ is the mean-free-path of the particles and L is the characteristic length scale. For neutral flow in a Hall thruster, L is typically the width or the length of the discharge channel. If we now assume the channel cross section is a pair of parallel plates extending to infinity in the azimuthal direction, a continuum flow in the Hall thruster can be described by the classic solution to the Poiseuille flow problem.[14] Much of the neutral flow in such a Hall thruster will still be developing while in the channel, but the flow at the exit plane should resemble the developed flow solution, which is given in Eq. (13),

$$u = u_{max}\left(1 - \frac{y^2}{h^2}\right), \; u_{max} = \left(-\frac{dp}{dx}\right)\frac{h^2}{2\mu} \tag{13}$$

where u is the axial bulk velocity, y is the radial coordinate with the origin on the channel centerline, h is half of the distance between the two walls, dp/dx is the axial pressure gradient assumed to be a constant for Poiseuille flow, and μ is the fluid viscosity. The solution takes on the form of a symmetric parabola with the maximum bulk velocity found on the channel centerline.

If, on the other hand, the flow is free molecular, the neutral particles only collide with the walls. The resulting velocity profile at the exit plane will depend on the geometry. Let the aspect ratio of the discharge channel be defined as channel length divided by channel width. The fraction of the neutral xenon that undergoes no collisions before exiting the thruster is 16% for a channel aspect ratio of 2 and 30% for a channel aspect ratio of 1. These numbers can be calculated by assuming the particles radiate out from the anode in a semi-circular manner. All other particles will interact with the wall before exiting the discharge channel. Assuming the extreme case where these interacting particles all thermalize with the wall, they will all exit the channel with roughly the same temperature and bulk velocity while the particles that do not interact will exit at anode temperature and their initial velocity. The resulting bulk velocity profile at the exit plane should be fairly flat, and the velocity distribution functions may be bi-modal if the wall and anode temperatures are sufficiently different.

III. Experimental Setup

Subsections A-E describe the LIF experimental setup.

A. Facility

Experiments were performed in the Large Vacuum Test Facility (LVTF) of the Plasmadynamics and Electric Propulsion Laboratory (PEPL) at the University of Michigan. The LVTF is a φ6 m × 9 m stainless steel-clad cylindrical chamber. Due to the size of the chamber, the thruster plume is able to expand un-impeded until termination at a beam dump ~4 m downstream. Pumping is provided by seven cryopumps with a nominal xenon pumping speed of 245,000 l/s. Facility pressure is monitored by two hot-cathode ionization gauges. The base pressure is approximately 2×10^{-7} Torr. The pressure during thruster operation at 30 mg/s anode mass flow rate is approximately 1×10^{-5} Torr, corrected for xenon.

During the experiments, the 6-kW Hall thruster was mounted on two cross-mounted stepper-motor translation stages. The stages provide 1 m of axial travel and 2 m of radial travel accurate to within 0.01 mm. Laser injection and LIF collection optics were fixed to the floor of the chamber.

Research-grade xenon propellant (99.999% pure) was supplied to the thruster by commercially available flow meters and controllers, having an accuracy of ±1%. Calibration of the flow system was done by the constant volume method taking into account the effects of compressibility.

B. Thruster

The 6-kW annular Hall thruster nominally operates at 300 V discharge voltage and 20 mg/s anode mass flow rate. Table 1 lists the operating conditions tested during this experiment. Note that the discharge voltage and anode mass flow rate are the main varying parameters between conditions. For the rest of this paper, operating conditions are labeled as YYY V, ZZ mg/s, where YYY is the discharge voltage and ZZ is the anode mass flow rate. Cathode mass flow rate is fixed to 7% of the anode mass flow rate for all operating conditions. Magnetic field settings are chosen to create roughly symmetric magnetic fields (about the thruster channel centerline) and to maximize thruster efficiency. These settings were found through the use of an inverted pendulum thrust stand.

Table 1. List of operating conditions.

Discharge voltage, V	Anode mass flow rate, mg/s
150	10
150	20
150	30
300	10
300	20
300	30
600	10

C. Laser and Air-Side Injection Optics

Figure 3 shows the air-side laser and optics setup for the LIF experiment. The laser system used is a TOPTICA TA-100/830 tapered-amplifier diode laser. This system has a nominal linewidth of ~10 MHz and a mode-hop-free range of ~12 GHz. Output power is ~250 mW at the wavelengths used in this study.

Two relatively weak beams are split off from the main laser beam and sent into the Burleigh SA-91 etalon assembly (2 GHz free spectral range, finesse >300) and the Burleigh WA-1000 wavemeter (accurate to 1 pm) for reference information. A third relatively weak beam is split off and sent into the optogalvanic cell for stationary reference. This beam is mechanically chopped at ~1.1 kHz.

The optogalvanic cell used in this study is a Hamamatsu L2783-42 XeNe-Mo galvatron. The core of the galvatron is a pair of φ6.25 mm cylindrical Mo tube electrodes centered in a φ25 mm x 120 mm glass cylinder. The cylinder is filled with approximately 3 Torr of xenon and 4 Torr of neon. The ends of the cylinder are angled at approximately 10 degrees from being perpendicular to the electrode axis to eliminate retro-reflection. The galvatron

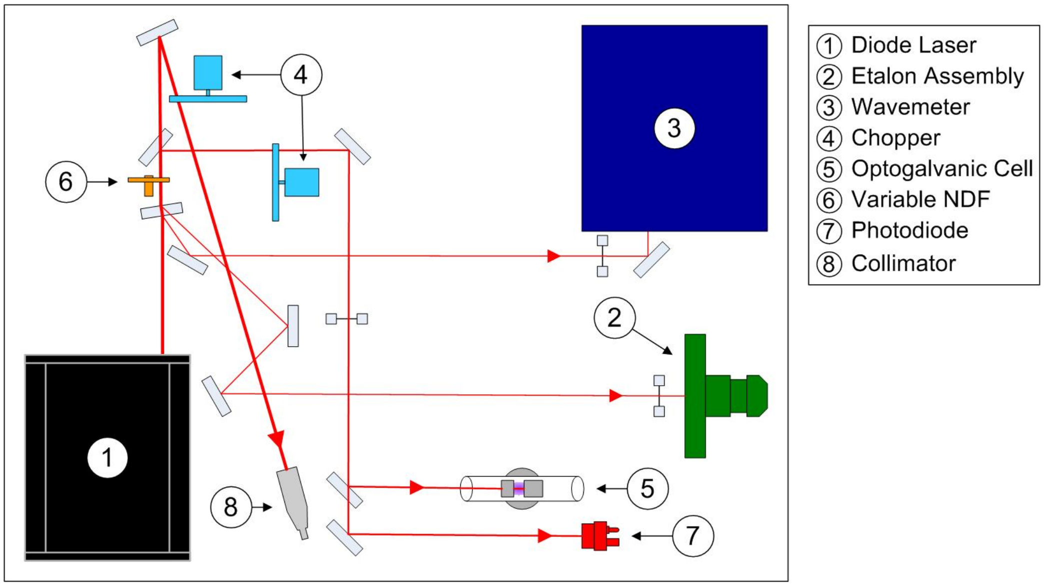

Figure 3. Air-side laser injection setup.

is operated at 250 V to maintain a warm, dense, and stationary plasma rich with ion species. The voltage drop across the cell's ballast resistor is connected to a SR-810 lock-in amplifier through an RC filter that passes only the AC component of the signal.

A fourth weak beam is split into a Thorlabs DET-110 photodiode to monitor laser power drift. This reading is fed into another SR-810 lock-in amplifier for signal collection. For a relatively unsaturated LIF trace, this laser power reading is used to remove the effects of laser power drift from the trace.

The remaining beam power is mechanically chopped at ~1.8 kHz via an SR540 chopper, and sent into a fiber collimator. The fiber delivers the light through an optical feedthru into the vacuum chamber.

When doing a saturation study, an additional variable neutral density filter is added so that the laser power being injected into the chamber can be fine tuned.

D. Vacuum-Side Optics

Figure 4 shows a diagram of the vacuum-side experimental setup. The injection optics sends the laser beam axially into the thruster. This beam is focused down to a point with a 1-mm diameter circular cross section via an anti-reflection-coated plano-convex lens. A polarizer (not shown in diagram) is placed between the optical fiber output and the lens to provide a horizontal polarization with respect to the chamber floor. The injection beam focusing cone has a half-angle of ~0.5° and the injection axis is aligned to within 0.1° of the thruster firing axis so cosine losses are negligible. The interrogation zone is at the 9 o'clock position when viewing the thruster face-on. To prevent excess beam drift during thruster operation an optical shield is installed to allow the laser to pass through while blocking the incoming xenon particles.

The collection optics is built from a matching pair of anti-reflection-coated achromatic lenses. Prior thermocouple measurements showed that thermal shielding is not necessary for the collection optics. Nevertheless, some thermal drift takes place over the course of the test so a reference pin is installed to the left of the thruster viewed face-on. The exact position of this pin relative to the thruster is known and the reflected laser signal from this pin is used to compensate for thermal drift.

For the Xe I 823.4 nm experiment, the collection optics is set at a 45±1° angle with respect to the thruster firing axis (Fig. 4a) to allow the interrogation of the inside of the thruster channel. This position is chosen based on a prior LIF setup that has been shown to collect good data.[15] The resulting intersection of the injection and collection optics forms a diagonally sliced cylinder ~1 mm in diameter in the radial direction and ~1.5 mm long in the axial direction. For the Xe I 834.9 nm experiment, the collection optics is set at a different angle to allow measurement all the way up to the anode. The collection optics is set at a 66±1° with respect to the firing axis (Fig. 4b). Since this position placed the collection optics closer to the thruster than in the previously proven configuration, the collection lenses were changed to allow a longer focal length. The interrogation zone for this second setup is ~1.5 mm in diameter. The size of the interrogation zone sets the spatial resolution of the LIF measurements.

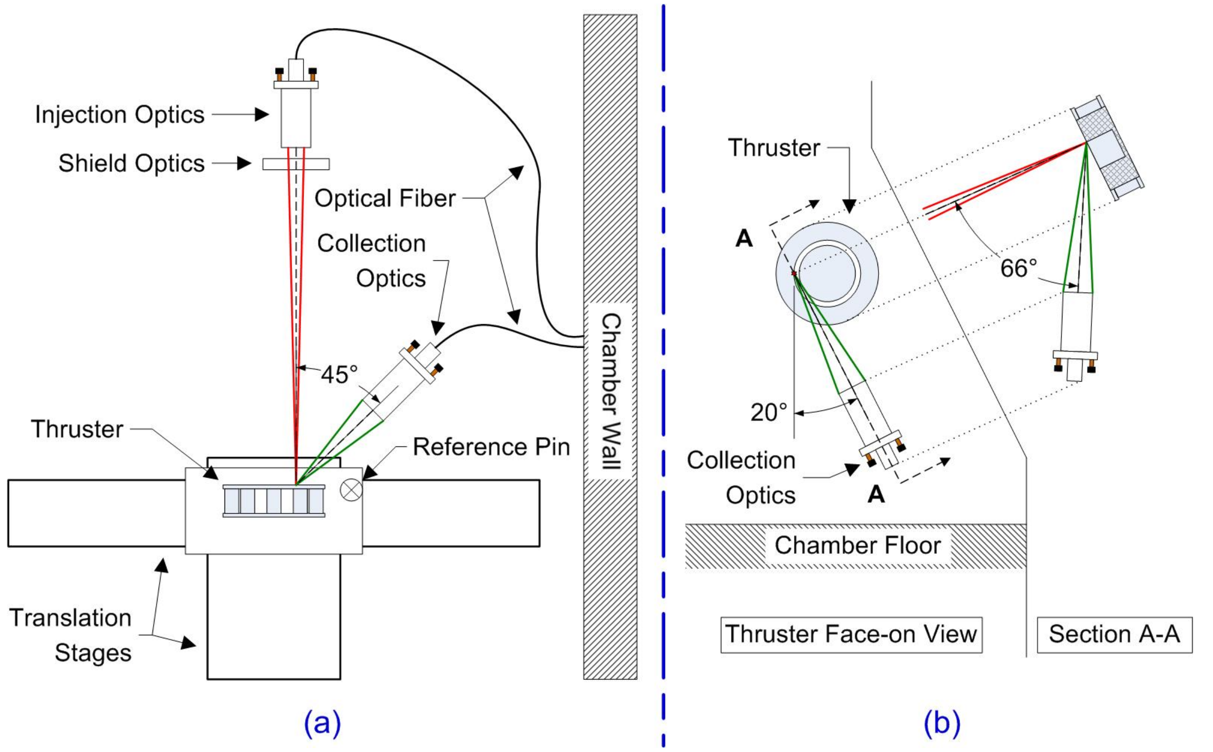

Figure 4. Vacuum-side experimental setup. *Sub-figure (a) depicts the setup for the Xe I 823.4 nm experiment. Sub-figure (b) depicts how the collection optics was re-positioned for the Xe II 834.9 nm experiment.*

E. Air-Side Collection Optics

An optical fiber brings the fluorescence signal from the chamber to a SPEX-500M monochromator, the output of which is amplified by a Hamamatsu R928 photomultiplier. The amplified signal is sent to a third SR-810 lock-in amplifier. A slit size of 1 mm, corresponding to an optical bandwidth of 1 nm, was used.

IV. Data Analysis and Results

A. Data Analysis

For the Xe I 823.4 nm experiment, parabolas are fitted to the main peak of the LIF and stationary reference lineshapes, then the difference in spectral frequencies is converted to equivalent velocity. Only data points with intensities greater than 70% of peak intensity are used in the curve-fit to guarantee that the fit is only applied to the main peaks. This method yields the peak velocity of the neutrals. Relative density is assumed to be proportional to the max intensity of the main peak based on the same curve-fit. Care is taken to make sure all data points for each set of relative intensity data are taken under the same equipment conditions. The main peak is ideal for relative density measurements because it is the most saturated of the four prominent peaks for this transition. Figure 5a shows the saturation study plot for the main peak. The region marked out by "operating regime" shows how little (±4%) the fluorescence intensity deviates as a function of laser power. The density of the lower state $6s[3/2]^0_2$ is dependent on a complicated set of interactions between various available states in a plasma and is usually a function of plasma temperature, density, and, by extension, collisionality. Usually, a collisional-radiative model is needed to correlate relative change in density of the excited state to the overall change in density of the neutrals. However, for a Hall thruster with a well-confined plasma, like the one found in the test article, the neutrals ionize very rapidly when it encounters the Hall current. So rapidly that the neutrals do not have time to come to a new thermal dynamic equilibrium. Thus any sudden change in the density of the measured excited state is a very good indication that the neutrals have arrived at the ionization zone. Due to limitations in the LIF setup and the transition, data are taken only near the exit plane, away from reflecting surfaces. The uncertainty associated with the peak velocity measurement is ±50 m/s. The uncertainty associated with the relative density measurement is ±20% due to the thruster geometry potentially blocking part of the collection optics view cone.

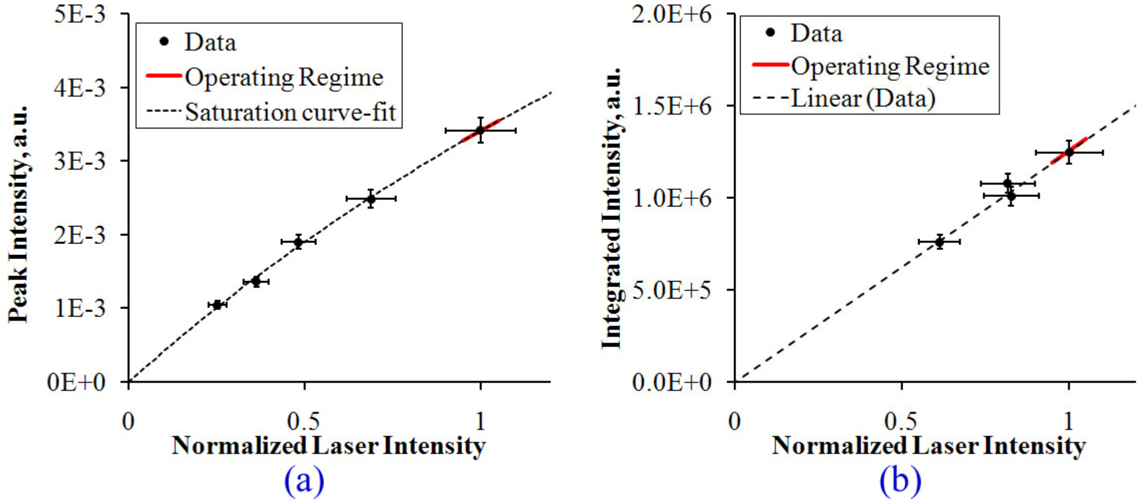

Figure 5. Saturation study plot for the Xe I 823.4 nm (left) and the Xe I 834.9 nm (right) experiments.

For the Xe I 834.9 nm experiment, it is found that the shift in frequency due to bulk particle movement is small compared to the frequency width associated with various broadening factors. The best way to obtain bulk velocity in this case is to perform direct averaging of the LIF and stationary reference lineshapes. This approach works for the second experiment but not the first because the LIF lineshapes are relatively unsaturated for the second experiment. Figure 5b shows the saturation study performed for the second experiment. Deconvolution of hyperfine structure lineshapes from the raw LIF lineshapes is carried out using Fourier transform with inverse Gaussian filter. This method is described in great details in Smith's work.[16, 17] Temperature measurements are calculated by first calculating the full-width-at-half-maximum (FWHM) velocity of the VDF, then finding a Maxwellian distribution whose temperature gives rise to the same FWHM velocity. This approach is useful because the VDFs are slightly non-Maxwellian with the majority of the distortion happening on the two wings of the distribution. The distortion in the wings can lead to erroneous temperatures if a simple Maxwellian fit is performed. For the most part, the data are taken from the anode all the way to the exit plane along the centerline. However, the signal tends to fall off quickly as the interrogation zone nears the exit plane. The resulting noisy traces produce large errors in bulk velocity and temperature and are discarded for the purpose of this study. This is why the Xe I 834.9 nm data set for most of the operating conditions do not extend all the way to the exit plane. For reported cases, the uncertainty associated with the bulk velocity is ±50 m/s. The uncertainty associated with the temperature range from 15-20% with the temperature of the wider (hotter) VDFs having lower uncertainty than that of the narrower VDFs. Only one set of representative error bars will be drawn for most plots to avoid clutter.

Note that all axial positions are normalized by the discharge channel length and negative axial positions are inside the channel. The exit plane is located at 0 and the anode is located at -1. Radial positions are normalized by the discharge channel width. The inner wall is located at 0 while the outer wall is located at 1.

B. Trends along the Thruster Channel Centerline

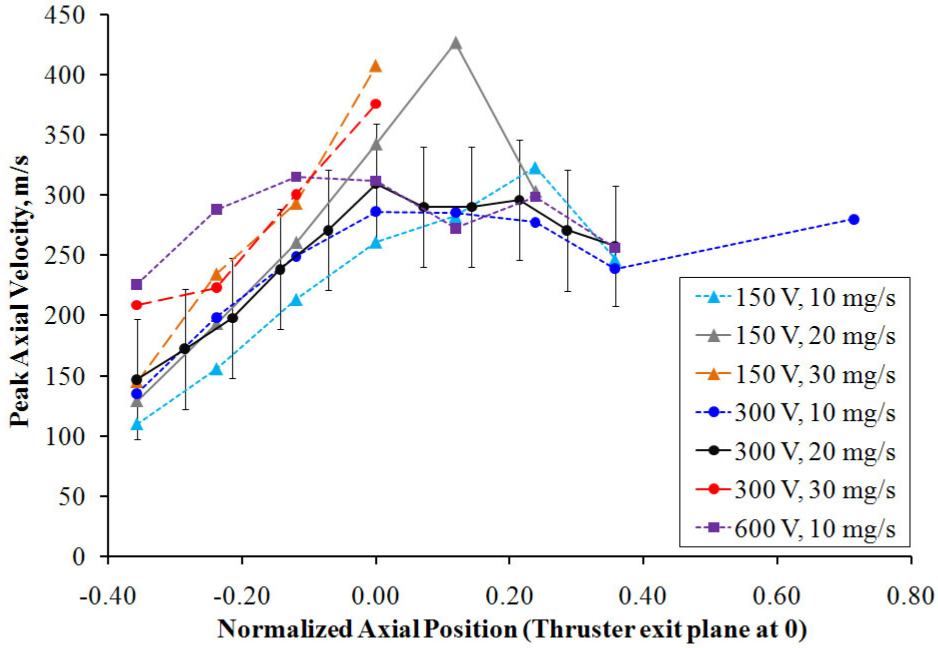

Figure 6. Peak velocity along the thruster channel centerline in the Xe I 823.4 nm experiment.

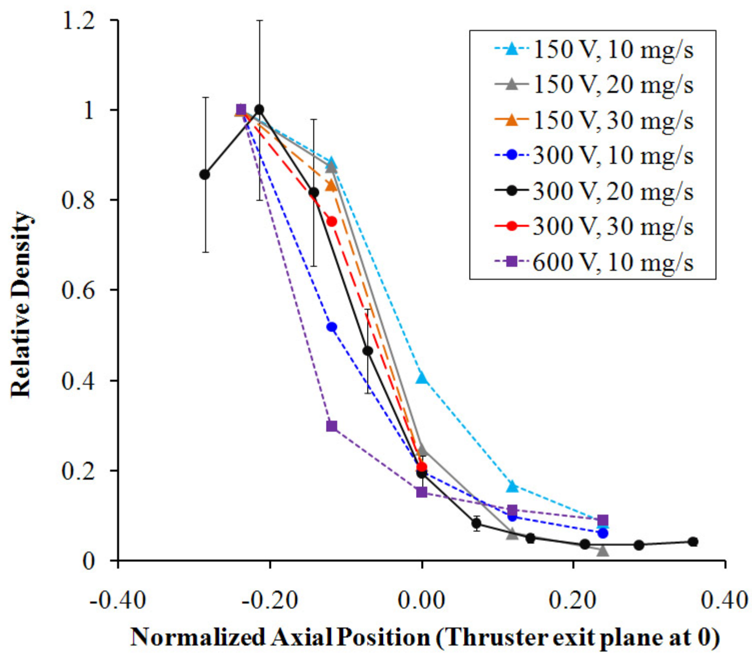

Figure 7. Relative neutral density along the thruster channel centerline in the Xe I 823.4 nm experiment. *Relative density is normalized against maximum recorded density for each operating condition.*

Figure 6 shows the peak velocity along the thruster channel centerline obtained in the Xe I 823.4 nm LIF experiment for the tested operating conditions. The data set stops at the exit plane for the two 30 mg/s conditions because the signal-to-noise ratio (SNR) became too low past the exit plane. In general, the neutrals increase in velocity as they approach the acceleration zone, which is found to typically center around the exit plane in a previous LIF study.[15] Figure 7 shows the relative density of the excited-state neutrals. Note that less data points are shown in Fig. 7 than in Fig. 6 because some LIF traces are believed to have been taken with the thruster blocking part of the collection optics view cone. While this obstruction does not affect peak velocity measurements, it does affect peak intensity and, by extension, relative neutral density measurements. The relative density is normalized against the maximum recorded density for each operating condition. The maximum is typically found at the furthest recorded upstream position suggesting that the density may further increase upstream. In general, the density drops by 1-2 orders of magnitude over a distance that is roughly a quarter of the discharge channel length. Although the lack of data further upstream makes our deduction less conclusive, we believe we have captured the general location of the ionization zone. Previous probe studies have shown that this thruster has a mass utilization of 90-95% across the listed operating conditions.[18] Given that the neutral velocity increases by a factor of ~2, the overall density must drop by roughly 95-97%, which matches well with the observed drop of 1-2 orders of magnitude in fluorescence intensity. The 10 mg/s cases may be an exception to this observation as the drop in relative density is smaller for these cases. Electrostatic probe data confirms that the ionization zone for the 20 and 30 mg/s cases are located at most a third of the discharge channel length into the channel from the exit plane. The probe data also suggest that the location of the ionization zone for the 10 mg/s cases is about halfway into the discharge channel.[18]

Figure 8 shows the velocity distribution functions along the channel centerline for the 300 V, 20 mg/s condition. In order to make the VDFs easier to distinguish from one another each lineshape has an offset of +0.2 a.u. with respect to the preceding lineshape on the legend list. The order of the legend is top down.

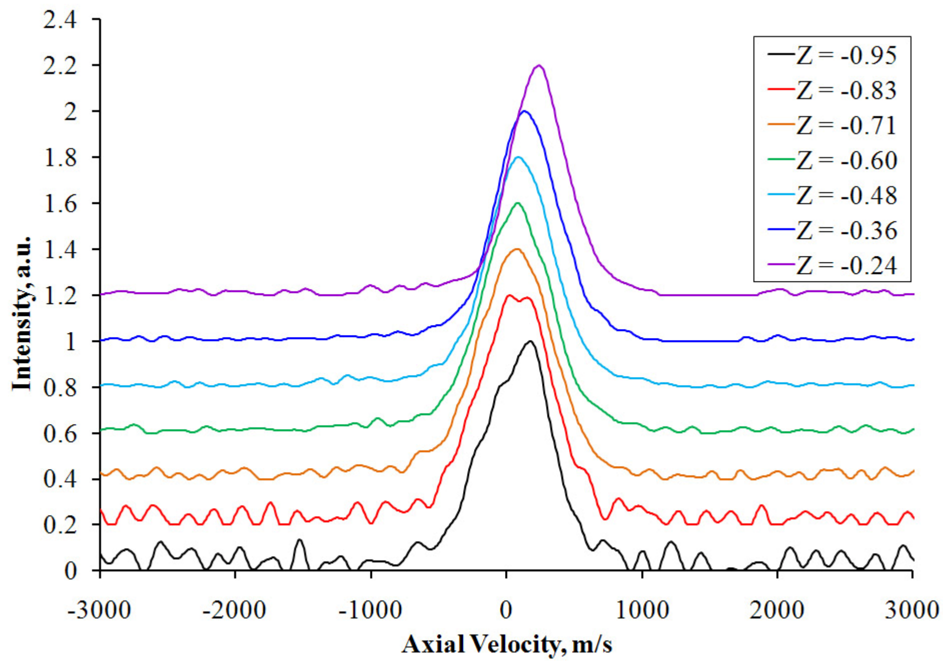

Figure 8. Velocity distribution functions along the channel centerline for the 300 V, 20 mg/s condition. *Z denotes normalized axial position with Z = -1 at the anode and Z = 0 at the exit plane. Each successive lineshape on the legend list (top down) is offset from the preceding lineshape by +0.2 a.u..*

Figures 9 and 10 show the bulk axial velocity and temperature results for the Xe I 834.9 nm LIF experiment, respectively. In general the neutral particles start out with bulk velocities of roughly 80-100 m/s across all conditions and gradually increase as they approach the bulk of the plasma at around the exit plane. Combining Figs. 6 and 9, we can see that the neutrals top out at around 300 m/s as they pass through the main plasma and appear to level off in velocity. There is no obviously discernible trend in the velocity with respect to the discharge voltage or the anode mass flow rate.

Somewhat surprisingly, the neutral temperature decreases as the neutrals flow downstream in the discharge channel. The neutrals start out at around 900-1600 K, which is similar to the anode temperatures we expect for this thruster. With the exception of the 300 V, 30 mg/s case, this temperature then spikes up by anywhere from 100 to 600 K depending on operating condition before gradually declining to 600-800 K near the exit plane. Due to low SNR, many of the data sets do not make it all the way to the exit plane where the bulk of the plasma is typically found. It is unclear whether the neutral temperature will increase again due to plasma heating. The SNR also tends to fall as one move far upstream into the channel because the thruster begins to obstruct part of the collection optics view cone. So the data found near the anode is noisier than the data found in the middle of the channel. The lower SNR may explain the spike in temperature near the anode though more extensive tests will be needed to confirm/disaffirm. There appears to be a trend where the temperature along the entire channel increases with anode mass flow rate. It is unclear whether the temperature correlates with the discharge voltage and the discharge power.

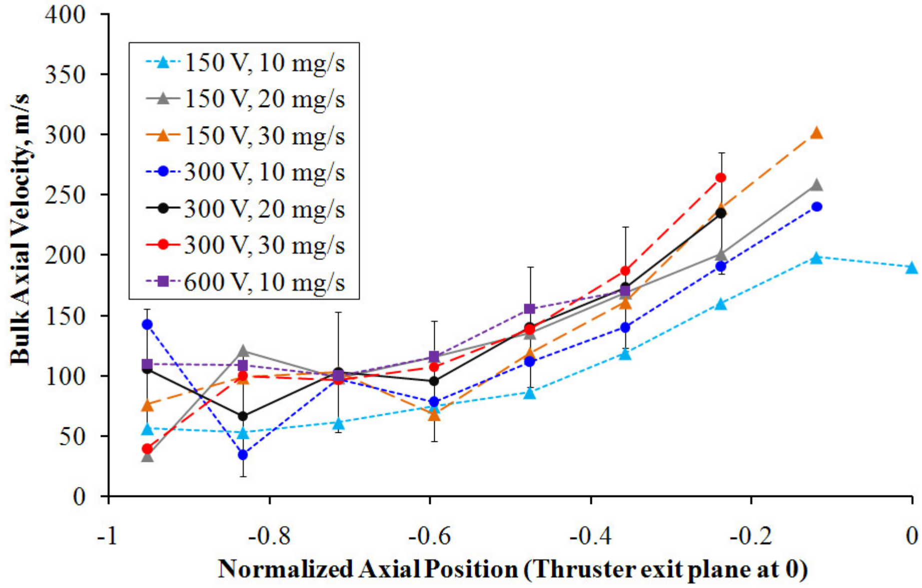

Figure 9. Bulk axial velocity along the thruster channel centerline in the Xe I 834.9 nm experiment.

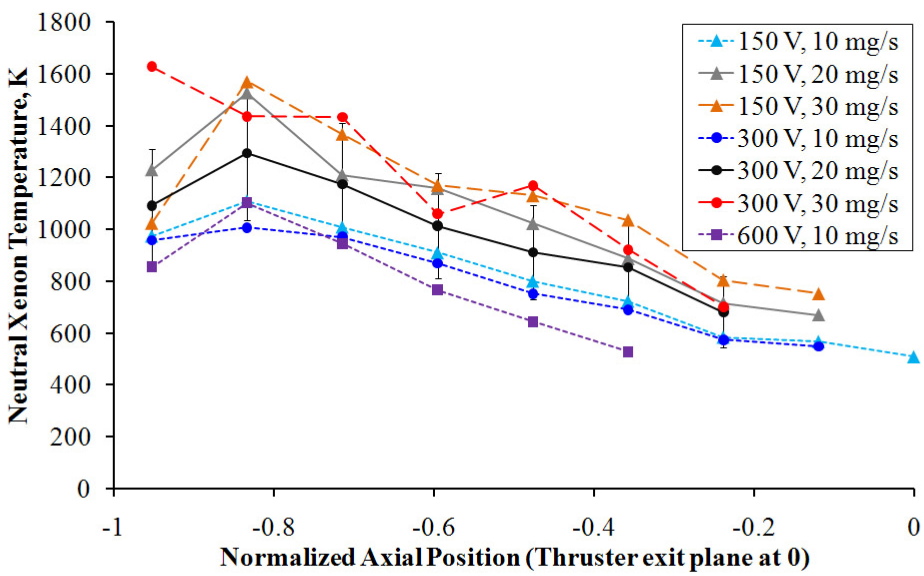

Figure 10. Neutral xenon temperature along the thruster channel centerline in the Xe I 834.9 nm experiment.

Figure 11 shows a composite plot of the velocity, relative density, and temperature data for the two experiments at 300 V, 20 mg/s. Also shown is singly-charged xenon LIF data from a previous study[15] pointing out the location of the acceleration zone and the bulk of the plasma. From this figure, we see that the majority of the Xe I 834.9 nm measurements are upstream of the main ionization zone. We can also see that the peak and bulk neutral velocity measurements from the two experiments agree fairly well given the expected uncertainty of ±50 m/s.

With Fig. 11, it becomes easier to see what kind of physical explanation will give rise to the observed velocity and temperature trends. There are a number of explanations for the acceleration and cooling of neutrals well ahead of the main plasma. The most obvious effect is the thermalization of the neutrals with the wall and themselves. In the free-molecular limit, the neutrals only collide with the wall. Since neutral xenon have a very high accommodation factor when striking boron nitride wall, they will leave with wall temperature most of the time. For this thruster, we expect a wall temperature of about 700-900 K with the exit being hotter due to plume impingement. As the initially slow neutrals collide with the walls, they transfer some of their thermal energy into the wall and gain thermal velocity associated with the wall temperature. For the expected wall temperature, mean thermal speed is 330-380 m/s, which is only slightly higher than the terminal velocity that the neutrals are observed to reach. This mechanism can also explain the observed cooling effect as the neutrals deposit thermal energy into the wall. In the continuum limit, there are still some wall effects, but the self-thermalization effect is expected to dominate. The hot but slow neutrals collide with each other and the resulting pressure causes expansion. These collisions lead to the conversion of thermal energy into directed kinetic energy due to the geometry of the channel. This self-thermalization effect is essentially a hydrodynamic effect. Although thermal energy is converted to directed kinetic energy in both limits, the physics behind the conversion is very different and can greatly affect how we should design the discharge channel if we want to minimize axial neutral bulk velocity in order to increase neutral residence time.

Another important explanation for neutral acceleration is simply that slower neutrals spend more time in the discharge channel than faster neutrals and are more likely to be ionized. This phenomenon, which will be called selective ionization for the remainder of this paper, can also contribute to neutral cooling. If we imagine a wide (high temperature) Maxwellian distribution and selectively remove the low velocity population, the distribution will become more narrow (low temperature) and is thus cooled. Given that neutral acceleration and cooling are observed well ahead of the ionization zone for 4 out of the 7 operating conditions, we conjecture that both thermalization and selective ionization are important for determining neutral velocity. Most likely, thermalization is more important at locations upstream of the ionization zone and selective ionization is more important in the ionization zone. However, it is the velocity with which the neutrals enter the ionization zone that, in principle, determines residence time and affects mass utilization. In that respect, accounting for thermalization may be more important than selective ionization when designing to maximize mass utilization.

A third explanation for neutral acceleration is charge-exchange effects. However, this effect is expected to be relatively small near the anode where there are few fast ions, and small near the exit plane due to the mean-free-path being longer than the channel length.

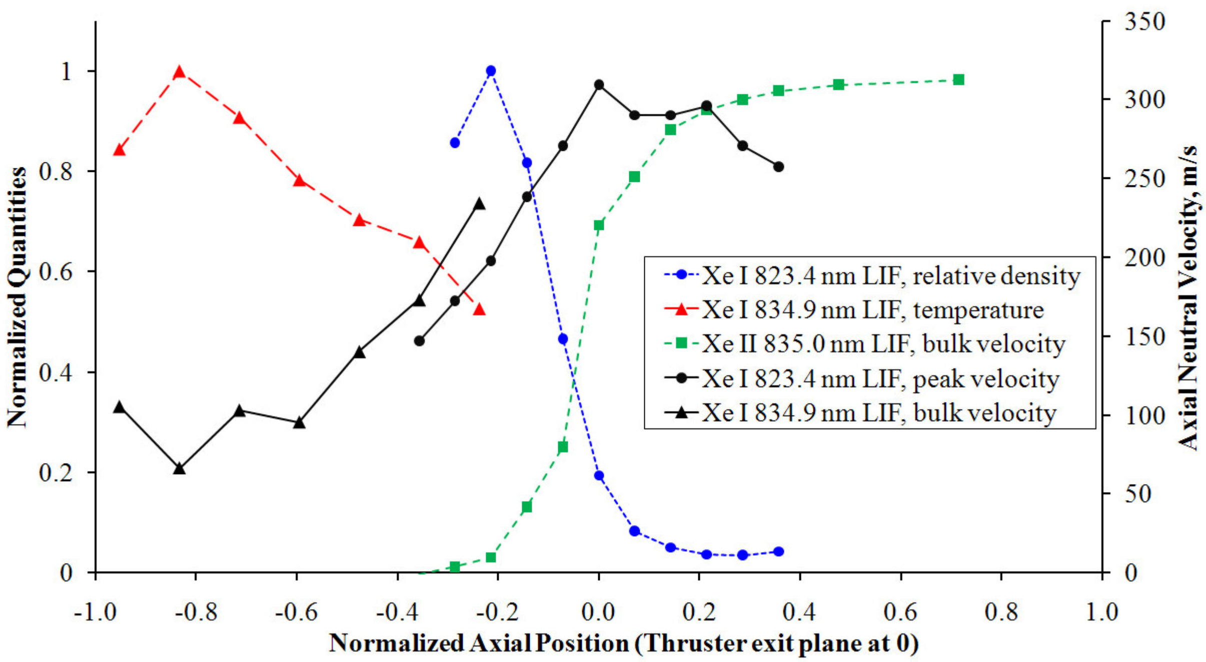

Figure 11. Composite data plot for the 300 V, 20 mg/s operating condition. *Density, temperature, and singly-charged xenon bulk velocity are normalized against their respective maximum recorded value (left vertical axis). Neutral bulk velocity and peak velocity measurements plotted using the right vertical axis.*

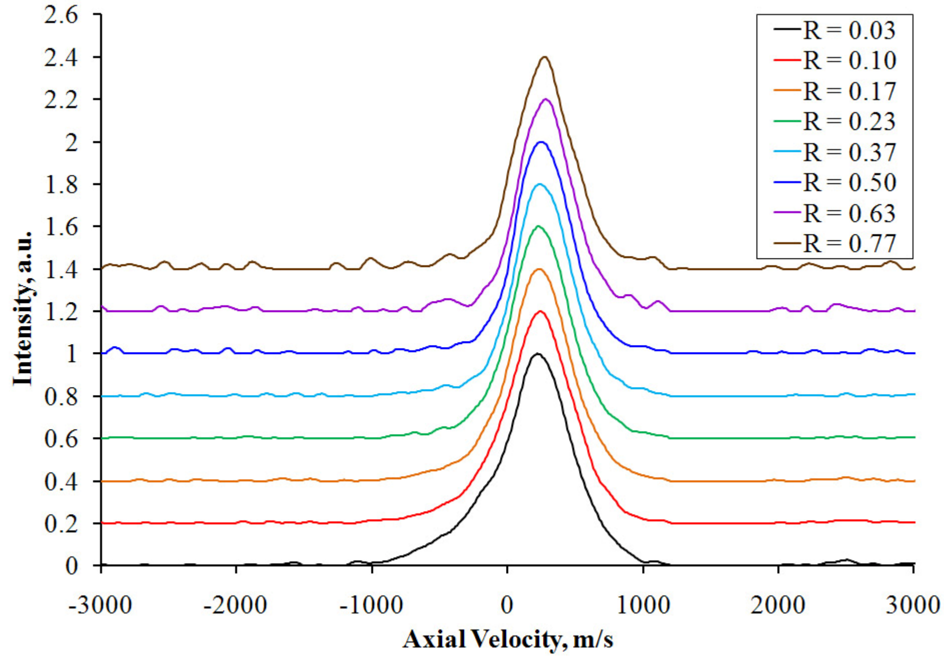

Figure 12. Velocity distribution functions across the thruster exit plane for the 300 V, 20 mg/s condition. *R denotes normalized radial position with R = 0 at the inner wall and R = 1 at the outer wall. Each successive lineshape on the legend list (top down) is offset from the preceding lineshape by +0.2 a.u..*

C. Trends across the Thruster Exit Plane

Figure 12 shows the velocity distribution functions across the thruster exit plane for the 300 V, 20 mg/s condition.

Figure 13 shows the data that we are able to collect for radial sweeps across the thruster exit plane at the 300 V,

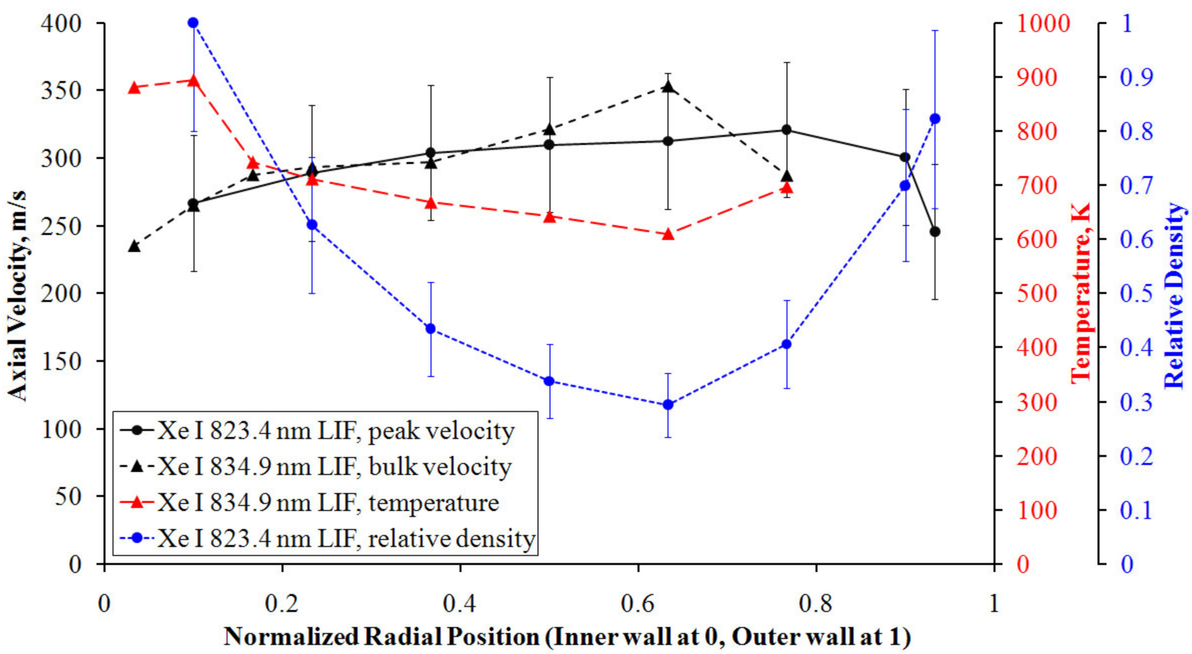

Figure 13. Peak and bulk axial velocity, temperature, and relative density of neutral xenon across the thruster exit plane at the 300 V, 20 mg/s operating condition.

20 mg/s operating condition. The Xe I 834.9 nm data set stops at around 80% across the width of the channel due to an unplanned thruster shutdown that happened while the next data point was being taken. Although not conclusive, the velocity seems to be lower and the temperature higher near the walls than at the center. The fact that the velocity profile is not a parabola but is slightly curved near the wall suggests the flow is transitional and there is some kind of neutral flow boundary layer very close to the wall. The temperature is higher near the wall than at the center most likely because at the exit plane the walls receive an especially large heat load from plasma impingement. The neutral density is over 3 times as high near the channel wall as in the center of the channel. This is most likely a result of the fact that the bulk of the plasma is confined toward the center and ionizes the neutrals that pass through the center more effectively. Note that the near-wall relative neutral density may be even higher since we could not quite reach the walls in our density measurements.

D. Flow Regime

From the data collected in this study, we can see trends that suggest the neutral flow exhibit some continuum behavior. One of them is the appearance of velocity and thermal boundary layers near the walls. Another is the fact that all VDFs obtained are very Maxwellian-like despite distortions that must be occurring due to selective ionization. This is only possible if collisional frequency is sufficiently high to allow some thermalization toward equilibrium. However, the velocity profile is not parabolic as a continuum Poiseuille flow should be.

There are also observed trends that suggest free molecular flow behavior. One of them is the relative flatness in the velocity and temperature profiles across the exit plane. Another is the distortions of various VDFs in the wings that represent deviations from Maxwellian distribution. On the other hand, there is the apparent presence of boundary layers that are not possible in purely free molecular flow.

Since the flow is most likely transitional, the best way to determine whether it is more continuum-like or more free-molecular-like is to calculate the neutral density and the Knudsen number. The neutral density can be obtained using Eq. (14),

$$n_n = \left(1 - f_i\right)\frac{(\dot{m}/m_{Xe})}{A_C < u >} \tag{14}$$

where n_n is the neutral density, f_i is the ionization fraction at the given location, $\dot{m}$ is the anode mass flow rate, m_{Xe} is the mass of xenon, A_C is the channel cross sectional area, $<u>$ is the bulk axial velocity. Note that if we had successfully mapped deeper into the discharge channel with the relative density measurements, we could have calculated f_i. Instead, we will only use Eq. (14) in the region upstream of where the ionization zone should reside and assume $f_i = 0$. This is justifiable as long as we are careful to use only data from upstream of where most of the ionization occurs. We restrict our calculations to the data points extending from the anode to halfway between the anode and the exit plane. Since the bulk axial velocity is relatively constant in this region, we will average the data points for each data set to obtain the neutral density. To calculate the Knudsen number we let L be the length of the channel and calculate the mean free path via Eq. (15).

$$\lambda = \frac{1}{\sqrt{2} n_n \sigma} \tag{15}$$

Where λ is the mean free path, $\sqrt{2}$ is to account for collisions between two particles of the same Maxwellian-like distribution, and σ is the collisional cross section. The van der Waals radius for neutral xenon is ~2 Å[19] so the cross section radius is ~4 Å. With the available information, we can further calculate the Reynolds number assuming continuum flow by using Eq. (16),[20]

$$Re = \frac{< u > L}{\beta_\mu < v_{th} > \lambda} \tag{16}$$

where L, the characteristic length, is once again the channel length, β_μ is a constant equal to 0.499 for monatomic gas, $<v_{th}>$ is the mean thermal speed calculated from the Maxwellian temperature, and λ is the mean free path.

Table 2 summarizes the results of the calculations. As expected, the neutral density increases with anode mass flow rate. The Knudsen number ranges from 0.23 to 1.02, which puts the flow regime right in the middle of being transitional. Reynolds numbers of around 1 suggest that the existence of neutral gas turbulence is very unlikely. And so plasma oscillations do not come from neutral gas turbulence in this Hall thruster. Note that the shape of the exit plane velocity profile (flat center with thin boundary layers at the edges) resembles the profile for a turbulent neutral flow between parallel plates. This explanation is invalidated by the non-existence of neutral flow turbulence.

Table 2. Calculate neutral flow properties

Discharge voltage, V	Anode mass flow rate, mg/s	Average upstream quantities		
		Density, m^{-3}	Knudsen number	Reynolds number
150	10	5.0e19	0.57	0.53
150	20	8.7e19	0.33	0.94
150	30	1.1e20	0.26	1.41
300	10	4.5e19	0.64	0.54
300	20	6.8e19	0.42	0.99
300	30	1.3e20	0.23	1.35
600	10	2.8e19	1.02	0.55

V. Discussion

There is currently debate about how much of a role charge-exchange (CEX) collisions play in the erosion of the Hall thruster channel walls. CEX collisions produce fast neutrals that are not bounded by electrostatic potentials and can cause great damage to the boron nitride walls. On the other hand, the CEX mean free path is typically longer than the channel length so there should be few of these fast neutrals compared to the number of impinging ions. All of this could change if there is a dense population of neutrals near the wall.

The LIF data in this study found that the neutral flow is slower and quite a bit denser near the wall. The near-wall neutral density may be high enough so that a fair fraction of the ions that would have otherwise missed the wall undergoes CEX collision and slams into the wall instead. Much more data will need to be gathered and simulations performed to see how much of a contribution to erosion fast neutrals really make. Future study in the area should concentrate on obtaining the neutral density and velocity vector along the channel wall.

As mentioned before, there are two neutral thermalization mechanisms both of which will accelerate the neutrals. Thermalization with the wall is more dominant for free molecular flow while self-thermalization is more dominant for continuum flow. Since the flow is transitional, both factors contribute to neutral acceleration. If one tries to cool the neutrals in order to decrease neutral velocity, increase neutral residence time and propellant utilization, it may be necessary to cool both the anode and the discharge channel walls.

VI. Conclusions

We have performed two LIF experiments examining xenon neutrals using the Xe I 823.4 nm and 834.9 nm transitions. In general, the particle velocity starts out at around 100 m/s at the anode and slowly rises up to 300 m/s at the exit plane. Equivalent Maxwellian temperatures calculated from FWHM velocity of the extracted VDFs show a cooling effect as the neutral particles move downstream. Relative density measurements show the general locations of the ionization zone. Several physical effects including thermalization and selective ionization are provided as possible explanations for the trends.

Radial sweeps across the exit plane revealed velocity and temperature boundary layers roughly a few mm thick for the 300 V, 20 mg/s operating condition. The neutral density was found to be at least a few times higher near the wall than at the center of the discharge channel for this operating condition. The possible existence of high-neutral-density boundary layers may provide support for the erosion of channel wall by fast neutrals born from CEX collisions.

The flow was found to be in the transitional regime. Calculated Knudsen numbers indicate the regime is about halfway between continuum and free molecular across all operating conditions. The nature of the flow suggests that the temperature of both the anode and the discharge channel walls may need to be controlled for a potential experiment to increase propellant utilization by reducing neutral flow velocity.

Acknowledgments

This research is funded by the Air Force Office of Scientific Research (AFOSR) grant FA9550-06-1-0105. The authors would like to acknowledge and thank the AFOSR and Dr. Mitat Birkan, the Project Manager, for this grant. The authors would also like to thank Dr. Tim Smith for his advice on laser-induced fluorescence.

References

[1]Reid, B. M. and Gallimore, A. D., "Langmuir Probe Measurements in the Discharge Channel of a 6-kW Hall Thruster", *44th AIAA/ASME/SAE/ASEE Joint Propulsion Conference & Exhibit*, AIAA-2008-4920, Hartford, CT, 21-23 Jul., 2008.

[2]Reid, B. M. and Gallimore, A. D., "Plasma Potential Measurements in the Discharge Channel of a 6-kW Hall Thruster", *44th AIAA/ASME/SAE/ASEE Joint Propulsion Conference & Exhibit*, AIAA-2008-5185, Hartford, CT, 21-23 Jul., 2008.

[3]Cedolin, R. J., Hargus, W. A., Hanson, R. K., and Cappelli, M. A., "Laser-Induced Fluorescence Diagnostics for Xenon Hall Thrusters", *32nd AIAA/ASME/SAE/ASEE Joint Propulsion Conference & Exhibit*, AIAA-1996-2986, Buena Vista, FL, 1-3 Jul., 1996.

[4]Hargus, W. A., Jr., "Laser-Induced Fluorescence of Neutral Xenon in the Near Field of a 200 W Hall Thruster", *41st AIAA/ASME/SAE/ASEE Joint Propulsion Conference*, AIAA-2005-4400, Tucson, AZ, 11-13 Jul., 2005.

[5]Hargus, W. A., Jr. and Cappelli, M. A., "Interior and Exterior Laser-Induced Fluorescence and Plasma Measurements within a Hall Thruster", *Journal of Propulsion and Power*, Vol. 18, No. 1, Jan.-Feb., 2002, pp. 159-168.

[6]Candler, C., *Atomic Spectra and the Vector Model*, 2nd ed. Van Nostrand, Princeton, N. J., 1964, pp. 313-315.

[7]Hill, E. L., "Relative Intensities in Nuclear Spin Multiplets", *Proceedings of the National Academy of Sciences*, Vol. 15, No. 10, 15 Oct., 1929, pp. 779-784.

[8]D'Amico, G., Pesce, G., and Sasso, A., "High Resolution Spectroscopy of Stable Xenon Isotopes", *Hyperfine Interactions*, Vol. 127, Aug., 2000, pp. 121-128.

[9]Suzuki, M., Katoh, K., and Nishimiya, N., "Saturated Absorption Spectroscopy of Xe using a GaAs Semiconductor Laser", *Spectrochimica Acta Part A*, Vol. 58, No. 11, Aug., 2002, pp. 2519-2531.

[10]Jackson, D. A. and Coulombe, M. C., "Isotope Shifts in the Arc Spectrum of Xenon", *Proceedings of the Royal Society of London. Series A, Mathematical and Physical Sciences*, Vol. 338, No. 1614, Jun., 1974, pp. 277-298.

[11]Harkness, H. W. and Heard, J. F., "The Stark Effect for Xenon", *Proceedings of the Royal Society of London. Series A, Containing Papers of a Mathematical and Physical Character*, Vol. 139, No. 838, 1 Feb., 1933, pp. 416-435.

[12]Ngom, B. B., Smith, T. B., Huang, W., and Gallimore, A. D., "Numerical Simulation of the Zeeman Effect from Laser-induced Fluorescence of Neutral Xenon", *30th International Electric Propulsion Conference*, 2007-254, Florence, Italy, 17-20 Sep., 2007.

[13]Karimov, R. G. and Klimkin, V. M., "Xe I and Xe II Radiative Lifetimes and Transition Probabilities", *Russian Physics Journal*, Vol. 14, No. 3, Mar., 1971, pp. 308-311.

[14]White, F. M., *Combined Couette-Poiseuille Flow Between Plates*, in *Viscous Fluid Flow*, 3rd ed. McGraw-Hill, New York, 2006, pp. 110-112.

[15]Huang, W., Drenkow, B., and Gallimore, A. D., "Laser-Induced Fluorescence of Singly-Charged Xenon Inside a 6-kW Hall Thruster", *45th AIAA/ASME/SAE/ASEE Joint Propulsion Conference & Exhibit*, AIAA-2009-5355, Denver, CO, 2-5 Aug., 2009.

[16]Smith, T. B., Ngom, B. B., Linnell, J. A., and Gallimore, A. D., "Diode Laser-Induced Fluorescence of Xenon Ion Velocity Distributions", *41st AIAA/ASME/SAE/ASEE Joint Propulsion Conference*, AIAA-2005-4406, Tucson, AZ, 11-13 Jul., 2005.

[17]Smith, T. B., "Deconvolution of Ion Velocity Distributions from Laser-Induced Fluorescence Spectra of Xenon Electrostatic Thruster Plumes", Ph.D. Dissertation, Aerospace Engineering, University of Michigan, Ann Arbor, MI, 2003.

[18]Reid, B. M., "The Influence of Neutral Flow Rate in the Operation of Hall Thrusters", Ph.D. Dissertation, Aerospace Engineering, University of Michigan, Ann Arbor, MI, 2008.

[19]Bondi, A., "van der Waals Volumes and Radii", *Journal of Physical Chemistry*, Vol. 68, No. 3, Mar., 1964, pp. 441-451.

[20]Vincenti, W. G. and Kruger, C. H., Jr., *Introductory Kinetic Theory*, in *Introduction to Physical Gas Dynamics*. Krieger Publishing Company, Malabar, Florida, 1965.